Mesocylindrical Aluminosilica Monolith Biocaptors for Size-Selective Macromolecule Cargos

S. A. El-Safty, M. A. Shenashen, M. Ismael, and M. Khairy*

Immobilization of biological macromolecules, such as protein, onto solid supports is an important method for diagnostic assays andgenetechnology. This present study reports the size-selective adsorption/removal of virtual proteins that have different shapes, sizes, functions, and properties, such as insulin, cytochrome c, lysozyme, myoglobin, β-lactoglobin, α-amylase, hemoglobin, and myosin in aqueous water using mesobiocaptor monoliths. To prevent large proteins from adsorbing and remaining attached to adsorbent surfaces, large, open, cylindrical-pored, three-dimensional cubic aluminosilica mesostructures with large aluminum contents and micrometer-sized monolith particles were fabricated. The unique physical properties and the surface functionality of the mesobiocaptors enhance protein adsorption characteristics in terms of loading capacity and quantity of the sample, ensuring a higher concentration of adsorbed proteins, interior pore diffusivity, and encapsulation in a short period. Thermodynamic studies indicate that protein adsorption into the mesobiocaptor pores is favorable and spontaneous. Theoretical models were used to investigate the major driving forces for the most optimal performance of the protein adsorption. The geometrical findings point to key factors, such as surface energy, intermolecular forces, charge distribution, hydrophobicity, and electrostatic interaction, which might control the adsorption into the interior large, open cylindrical mesobiocaptor cavities (sized 3–16 nm) without aggregation of these proteins on the exterior surfaces of monoliths. Indeed, the availability of adsorption of single proteins from mixtures based on size- and shape-selective separation opens new avenues of research in encapsulation of proteins and bioanalysis.

1. Introduction

With the remarkable progressin the field ofgenetechnology, proteins have an important place in the field of disease diagnosis and treatment.[1–6] The arrival of protein at the interface is driven solely by diffusion processes that are dependent on bulk concentration and diffusion coefficients, resulting in frequent collisions.[6] In particular, thanks to its low maintenance costs, high efficiency, and ease of operation, adsorption has proven to be one of the most attractive and effective techniques. The uptake of protein on the substrate follows a complex mechanism that involves many events, such as conformational changes, hydrogen bonding, and/or hydrophobic and electrostatic interactions. Protein adsorbs in different qualities, conformations, and orientations, depending on the chemical and physical characteristics of both the protein and the supported surfaces.[7,8] Many studies use several nanostructures for the targeted separation of biomolecules from biosamples, such as, nickel oxide, multifunctional magnetic nanorods, and different core/shell and porous materials.[1–4]

Furthermore, biomedical and nanotechnological applications increasingly use interfaces between inorganic material and polypeptides in various scientific fields, such as nanobioscience, material science, artificial implant, protein-purification strategies, biosensors, drug delivery systems, catalysis, catalysis support, and molecular biology/biotechnology.[9] Several kinds of materials with different retention mechanisms have been developed to improve the efficiency and specificity of solid-phase extraction, such as conventional chromatographic separation materials,[10,11] magnetic beads,[12] and organic and inorganic polymers[13] with reversed-phase or ion-exchange groups. With the remarkable developments in the area of nanotechnology in the last few decades, hieratical mesoporous structures are highly desirable materials that have a large surface area, high porosity with uniform and tuneable mesopores, hydrophilic character, and relatively good chemical and mechanical stability in light of changes in the microenvironment.[14–19] These features make mesoporous materials good substrates for hosting catalysts, adsorbing proteins, constructing biosensors, separation sensors, and fuel cells.[2,15,16,19] Functional metal nanoparticle (NP)-supported mesoporous oxide powder hosts enhance potential activities because of their high surface area and continuous pore structure. Xu and Gao mentioned that different functional proteins are able to bridge SiO_2 nanoparticles via charge attraction and hydrogen bonding, thereby aggregating them into coralloid forms.[14]

However, the main challenge of designing mesostructures capable of macromolecule immobilization and uptake into the

Prof. S. A. El-Safty, Dr. M. A. Shenashen, Dr. M. Ismael, M. Khairy
National Institute for Materials Science (NIMS)
1-2-1 Sengen, Tsukuba-shi, Ibaraki-ken 305-0047, Japan
E-mail: sherif.elsafty@nims.go.jp
Prof. S. A. El-Safty, M. Khairy
Graduate School for Advanced Science and Engineering
Waseda University, 3-4-1 Okubo, Shinjuku-ku
Tokyo 169-8555, Japan; E-mail: sherif@aoni.waseda.jp

DOI: 10.1002/adfm.201200393

interior mesoporosity remains. To control the design of macromolecule biocaptor-based mesostructures, uniform and tunable pore sizes play a crucial factor for protein penetration into mesopore cavities. Mesoporous silica (SBA-15) molecular sieves have shown high ability to immobilize α-amylase without considerable protein leaching.[19] Among all mesostructures, three-dimensional (3D) pore cavities have been receiving much attention as superior materials compared to one- or two-dimensional structures, such as MCM-41 and SBA-15, in terms of mass transfer and pore blocking.[15] Furthermore, biocaptors with functional acid sites or positively charged surfaces display a greater probability for hydrophobic interactions of protein.[8]

We have fabricated nanofilter-based hexagonal mesocylinders or cage pores inside anodic alumina membrane (AAM) nanochannels for promising size-exclusion separation of proteins;[20] however, size-selective adsorption of low-molecular-weight proteins into uniform, large mesopores could lead to their applications in encapsulation of proteins and bioanalysis.[21] In addition, the preparation of very active and stable biocaptors with appropriate dynamic working ranges and cycles, large pore sizes, and multidirectional geometries is a key requirement in successful protein immobilization and uptake. Due to tendency for large proteins, particularly at high feed concentration, to adsorb and remain attached to adsorbent surfaces, fabrication 3D cubic mesostructures with large, open, cylindrical pore cavities that have actively interior function sites for ensuring encapsulation of size-selective proteins is highly desirable in this field.

In the current study, we report a simple yet general approach for the fabrication of 3D cubic mesobiocaptor aluminosilicas with large, open, cylindrical pore cavities (sized 3 nm to 16 nm) and micrometer-sized monolith particles. The physical features and active acid sites of monoliths function as mesobiocaptors that can rapidly (in minutes) encapsulate large quantities of biological proteins into the cylindrical cavities. To the best of our knowledge, the present report is the first to provide geometrical models of the 3D mesobiocaptors that involve the major driving forces for the most optimal encapsulation/adsorption performance in terms of diffusivity and quantity, particularly with large molecular weight, size, and concentrations of proteins. Indeed, the availability of adsorption of single proteins from mixtures based on size- and shape-selective separation might open up new avenues of research in encapsulation of proteins, bioanalysis, and drug delivery systems. Moreover, the retention of mesobiocaptors enables a controlled encapsulation/immobilization process that involves the evaluation of manufacturability of adsorbents in terms of reusability and high capital tolerances.

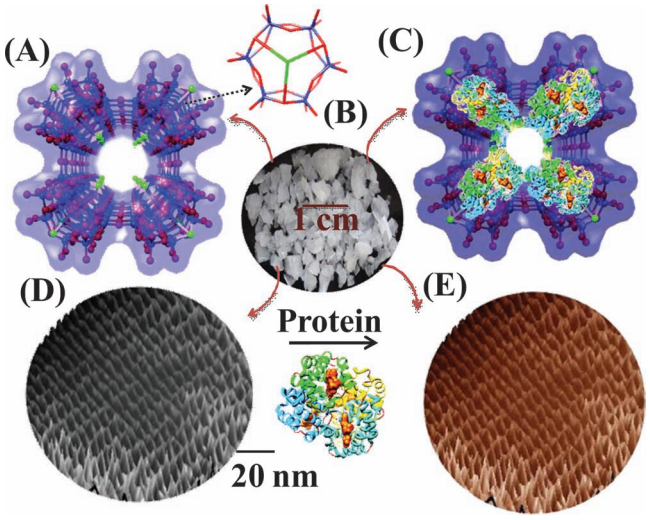

Scheme 1. 3D Geometrical models (A,C) and pore surfaces (D,E) of mesobiocaptors based on cubic *Pm3n* mesostructures with aluminosilica cylindrical pore monoliths (B). The design indicates the feasibility of the protein adsorption interior mesopores (C) and inside pore surfaces (E) of 3D cubic *Pm3n* aluminosilica structures with Si/Al ratio of 4. The colors of the atoms in the truncated aluminosilica cluster (A) are as follows: Al (green), Si (Blue), and oxygen (red), respectively.

2. Results and Discussion

2.1. Synthetically Constructed Cubic Pm3n Mesobiocaptors

The development of a new strategy to synthetically construct cubic *Pm3n* mesostructures with large, tunable, and open cylindrical pores (3–16 nm) is therefore highly desirable to trap large biomolecules, such as proteins (**Scheme 1**). This stirring-assisted synthesis approach has several key advantages: (1) the ability to control enlargement of regular mesocylindrical pores, even with high Al contents of mesobiocaptor aluminosilica monoliths; (2) the alumina/silica precursors are homogeneously distributed in all the structure matrices, thereby preventing formation of irregular bubbles or empty spaces that would traduce into undesired voids in the final space confinement monoliths (Scheme 1D and 1E); (3) quaternary microemulsion liquid crystalline phases of Brij 58/C_{12}-alkane/TMOS/H_2O-HCl/ethanol composition are used to control engineering pore systems with primitive-centered cubic *Pm3n* structures, as evidenced from XRD and HRTEM profiles (**Figure 1** and **2**);

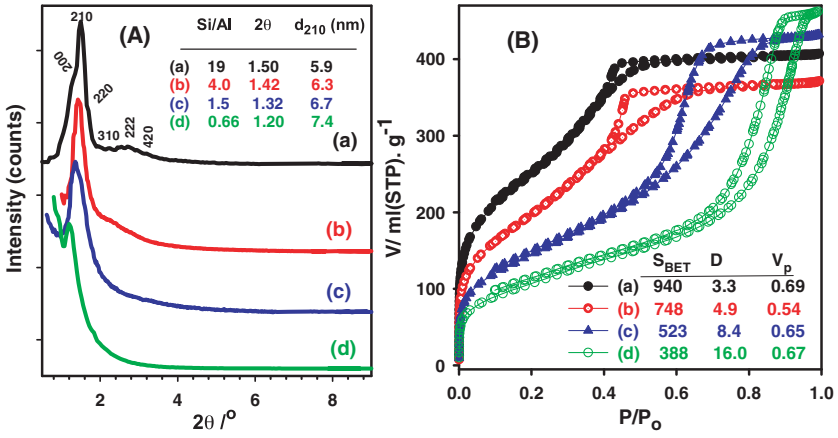

Figure 1. XRD (A) and N_2 isothermal (B) patterns of meso-cage cubic *Pm3n* (a-d) aluminosilica biocaptors with Si/Al mole ratios of 19 (a), 4 (b), 1.5 (c) and 0.66 (d) that fabricated in microemulsion systems of Brij 58 at Brij 58/TMOS ratio (w/w) of 0.5. Inserts (B) are S_{BET} (m^2/g), D_{NLDFT} (nm), Vp (cm^3/g).

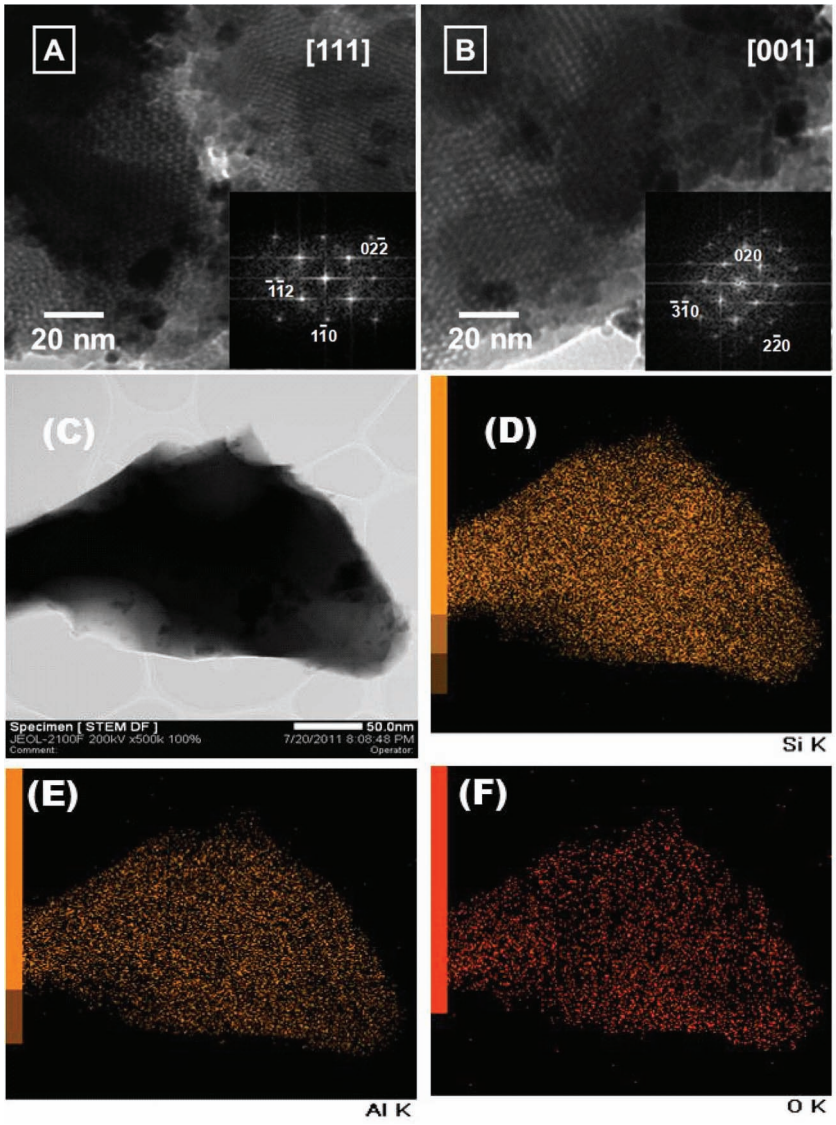

Figure 2. Representative HRTEM micrographs and FTD (insets) patterns of cubic *Pm3n* aluminosilica mesobiocaptors with Si/Al mole ratios of 19 (A,B). HRTEM and FTD patterns of cubic *Pm3n* were recorded along the [111] (A), and [001] (B) zone axes, respectively. (C-F) STEM-EDS mapping of the aluminosilica monoliths; (C) Dark-field STEM image of monoliths, STEM-EDS mapping of (D) silica, (E) alumina and (F) oxygen.

and (4), despite the stirring conditions, these mesocylinderical aluminosilica retain well-defined micrometric morphology of monoliths, thereby opening up new ways to realize micro-objects tailor made to a given protein encapsulation design. Due to the morphological defects, particularly with the Al content samples, irregularly shaped intrapore voids (distributed between 100 nm and 1 μm) are formed (see Supplementary Figure S1). The development of ultra- or micrometer-size-scale morphology composed of 3D tube-shaped mesoporous monoliths that could effectively separate large macromolecules, such as myosin, would greatly assist in other potentials for biomedical applications.

The molecular engineering model of the 3D cubic *Pm3n* network clusters may be the key to the precise manipulation of encapsulation/immobilization process of protein (Schemes 1A and 1C). The particular shape and connecting pores with columnar *Pm3n* phase domains might render the size-selective adsorption of protein into interfaced cavities to be more easier. In addition, the large molecular masses and the density of functional groups of aluminosilica octahedral (O_h) clusters connected in 3D cubic network structures are vital and important to the development of efficient mesobiocaptors. In this way, the structural-ordering features of cubic *Pm3n* phase architectures are combined with the ability for distinct protein adsorption that corresponds to the pore diffusivity (Schemes 1D and 1E).

Scheme 1A shows the 3D cubic *Pm3n* molecular networks assembled from the connection of aluminosilica octahedral (O_h) clusters. Analysis of the truncated aluminosilica cluster reveals high symmetry with the composition of $Al_3Si_{12}O_{30}$ or $AlSi_4O_{10}$. The truncated octahedral structure is based on orientation of the oxygen atoms around the main axis passing through the Al. Generally, two types of oxygen linkages exist: oxygen-bridge Si or Al and siloxane species. The first group has Si-O bond distance of 1.65 Å, whereas the bond distance of the siloxane groups is 1.61 Å. Each octahedron cluster shares a face with another via siloxane groups through linear extension, generating eight irregular faces. The Al atom is coordinately bound to the oxygen, forming a C_2 axis of symmetry with Al (Al distance measuring 3.81 Å). This cluster orientation results in open, nanoscale, cylindrical network pores. Schemes 1C and 1E show the stability of the orientational mesobiocaptor pores after immobilization of the proteins (see below).

2.2. D Biocaptor Networks with Mesocylinder Hierarchical Structures

The XRD profiles of the calcined mesoporous aluminosilica (**Figure 1**A) reflect the high quality of the materials. The diffraction peaks provide evidence that the ordered primitive-centered cubic *Pm3n* structures are characteristic of the fabricated monolith biocaptors (Figure 1A).[27,28] Despite the high loading level of adsorption of protein molecules into the pore surface, finely resolved Bragg diffraction peaks are clearly evident for the cubic *Pm3n* biocaptors with Si/Al ratio of ≤ 4 (Figures 1A-a and 1A-b). Retention of the mesoscopic orientation order of biocaptors might lead to successful adsorption of different adsorbates, especially protein molecules, into the condensed framework pore matrices of the 3D cubic mesostructures. However, the stability of the mesoporous matrices, even with high Al contents (Figures 1A-c and 1A-d) increases the possibility of high

flux and uptake of protein adsorption process (see below). In turn, the partial collapse of mesostructures may be due to a lack of long-range crystallographic order or to the finite size effects of Al-SiO_2 inside the mesopore structures, as evidenced from the low-intensity reflections with high Al contents.[29,30] Two key findings from the increased the unit-cell constants of the cubic *Pm3n* structures ($a_{pm3n} = d_{210}\sqrt{5}$) with increase in the Al contents were as follows: (1) the high aluminum salt in the composition synthesis domains might change the micellar aggregate sizes and volume fractions of the sphere core and the corona of the Brij 58 ($C_{16}EO_{20}$) surfactant at specific synthesis compositions,[30] (2) the addition of swelling agent (C_{12}-alkane) and cosurfactant (ethanol) under stirring-assisted synthesis leads to the formation of large, open cylindrical mesostructures.

A high specific surface area and meso–macroporous hierarchy are required for the immobilization of elevated proteins. The nitrogen adsorption–desorption isotherms for the different *Pm3n* monoliths samples showed type-IV behavior as per IUPAC classification and pronounced hysteresis loops of H_1 types with well-known sharp inflection of the adsorption/desorption branches featuring uniform and open cylindrical pore architectures (Figure 1B).[27,31,32] These results can be attributed to capillary condensation taking place within a narrow range of tubular pores. Under this stirring-assisted microemulsion system, increases of aluminum content significantly led to a shift of adsorption/desorption isotherms toward a higher relative pressure (*P*/*Po*). The lower closure point of the hysteresis loop was significantly depended on the Al content; this indicates the columnar-induced stepwise desorption in the open tubular pores, leading to more easier diffusion, particularly for large macromolecules, such open tubular-like pore scaffolds, than that of ink bottle pore materials with narrow entrances.[33,34] Based on the N_2 isothermal results, the physical characteristics of the cubic *Pm3n* monoliths, such as large porosity, specific surface area, and pore volume, allow the protein molecules to access the monoliths. The large increase in the cylindrical mesopore cavities of biocaptors may be attributed to the instability of aluminum in the frameworks and the stirring-assisted conditions. In fact, homogenous diffusion and rapid transport of protein molecules onto the ordered pore networks lead to excellent adsorption in a short period. In addition, the direct fabrication method of biocaptors offers a wide range of pore sizes, leading to the immobilization of a sizeable number of macromolecules.[35]

TEM images of cylindrical cubic *Pm3n* aluminosilica monoliths (with Al/Si ratios of 19) recorded along [111] and [001] directions reveals evidence of well-ordered pores connecting to large regions of cubic *Pm3n* aluminosilica monoliths (**Figure 2**A and 2B). These images show uniformly sized pores arranged with cubic *Pm3n* lattice symmetry. FTD patterns (insets) provide more details on the primitive-centered cubic symmetries according to the abundance of lattice fringes. Arrangement of planes in these specific lattice fringes along the [111] and [001] zone axes provide further evidence of the formation of ordered cubic *Pm3n* lattice symmetry.[37] Despite the decrease of long-range structural ordering of cubic lattices with Si/Al ratios as high as 1.5, these mesobiocaptors show a high degree of mesoscopic pores, consistent with their XRD and N_2 profiles.[21–23,35,36]

Further evidence for the formation of well-distributed mesoporous aluminosilica monoliths under the stirring-assisted approach is revealed by the STEM images (Figure 2C and 2D). The dark fields in the STEM images confirm the formation of nanoscale monoliths. The morphology and the EDS mapping of mesobiocaptor were further characterized using STEM and STEM-EDS, as shown in Figure 2C–2F. In order to characterize the surface composition and atomic distribution of mesoporous alumina, STEM-EDS mapping was carried out. The STEM-EDS map of aluminosilica mesostructure exhibits the presence of Si, Al and O (Figure 2D–F). However, the contribution of O and Si and Al are mainly from mesostructure (Figure 2C). The STEM-EDS mapping also indicates that Si, Al, and O atoms are uniformly distributed in the mesobiocaptor aluminosilica, leading to homogenous diffusion of the proteins into this mesobiocaptor monoliths.

2.3. Surface Acidity and Composition of Mesobiocaptors

To investigate the pore surface acidity of mesobiocaptors, atomic charge distributions of 3D cubic *Pm3n* network clusters for 12 units of $AlSi_4O_{10}$ composition were calculated using the semiempirical PM3 method implemented on HyperChem 8.0.7 program package (developed by Hypercube, Inc.) (**Scheme 2**). Note that the Si/Al ratio used in this cluster was 4 (see supplementary Table S1). The existence of Al_2O_3 nodes at the edges of the truncated aluminosilica clusters created functional acid sites at the ends and inside the pore walls. Results show that the oxygen atoms in the Si–O–Al linkages were more negative than other oxygen atoms in the linkage species, pointing to the high acid sites. In addition, the Al atoms had different charges depending on their position on the surface or towards the pore. According to our calculations, Al charges were 1.89 and 1.82 on both the surface and pore, respectively, leading to creation of Brönsted and Lewis acidity, as evidenced from NMR and TPD analyses (see supplementary Figure S2 and Figure S3).

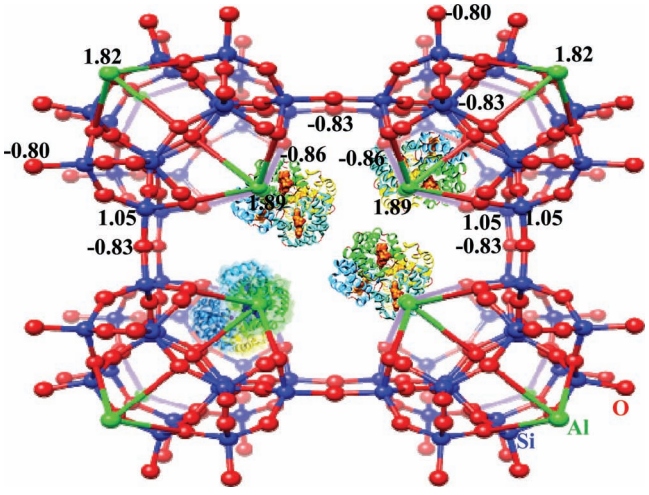

Scheme 2. Atomic charge distribution of 3D cubic *Pm3n* network cluster units of aluminosilica mesobiocaptors. Note that the Si/Al ratio used in this clusters is 4.

To confirm the presence of surface acidity of the guest-free samples, ^{27}Al NMR and NH_3-TPD were measured (see supplementary Figure S2 and Figure S3). Three ^{27}Al peaks centered at chemical shifts of –1, 37 and 58 ppm, indicating the existence of octahedral (Al^{VI}, AlO_6, and extra framework), pentahedral Al^{V}, AlO_5, and extra framework) and tetrahedral (Al^{IV}, AlO_4, and framework) aluminum sites, respectively. The formation of the coordination state of the aluminum species in four-, five-, and six-coordinate environments indicates the existence of different bonds between Al, O, Si, and H. The coordination and location of aluminum sites in the frameworks were key determinants in the generation of surface acidity in the aluminosilica samples. The ^{27}Al MAS NMR spectrum result clearly indicates that the aluminum was mainly incorporated into the mesoporous framework, as evidenced by the EDX analysis (see supplementary Figure S1).

The NH_3-TPD results show two main peaks of NH_3 desorption around 200 °C and a small, broad peak at 200–500 °C, indicating the formation of the weak "Lewis" and mildly strong "Brönsted" acid sites of the OH-groups of aluminosilica mesobiocaptors (see supplementary Figure S3). To determine quantitatively the amount and strength of acid sites, the peaks around 100 °C to 500 °C were deconvolved using a Gaussian function, with the temperature as the variant. The number of acid sites increased with the amount of aluminum in the monoliths, leading to the formation of interaction sites for the biomolecules.

2.4. Batch Adsorption Assays of Macromolecules

Several key factors, such as molecular shape and size, concentration, and composition of proteins, in addition to the amount of active surface sites of aluminosilica adsorbents, were investigated in the adsorption assays (**Figure 3**A to 3C). To study the effect of active surface sites of mesocylindrical biocaptors on the performance of protein size-selective adsorption into the internal pores, a series of Mb (1×10^{-5}M) adsorption assay was performed using biocaptors synthesized with different Si/Al ratios (from 19 to 0.66) (Figure 3A). Due to the performance of the adsorption assays in water, all Lewis acid sites might transform into Bronsted acid sites of the aluminosilica mesobiocaptors. Therefore, the number of Bronsted acid sites for mesobiocaptors is the key factor for the enhanced adsorption uptake with high Al contents. The natural surfaces of these acid sites strongly induce the H-bonding and dispersive interactions with biomolecules inside the interior pores (Scheme 1C).[37,38] This finding indicates that the biomolecules may be readily adsorbed into monoliths with large numbers of aluminum sites.

Protein molecular size and concentration play significant roles in the efficiency of mesobiocaptors in terms of the large-quantity and high-speed adsorption of proteins or any biomolecules. Figure 3B shows the adsorption assays with different protein sizes and molecular weights such as INS, CytC, LYS, Mb, β-LG, Hb, AMY, and MYS, and at various concentration ranges of Mb protein using mesobiocaptors with Si/Al ratio 0.66 and with large cylindrical pore size of 16 nm. This adsorption assay had three characteristics: (1) induced adsorption period in the order of minutes, depending on each protein molecular weight, shape and size, was clearly distinct; (2) the adsorption rate was significantly increased with the increase of time; and (3) the saturation of the adsorbed amount at the equilibrium state was observed in such S-adsorption curves. Results reveal that the adsorption rate and capacity increased with decreases in protein molecular weight and size and concentration (Figure 3B and 3C). To investigate the feature of adsorption efficiency in terms of rate and capacity and stability of protein immobilization into the interior pores of mesobiocaptors during the adsorption assays, kinrtics and thermodynamic study were conducted on protein bioadsorption at different temperatures at 25–40 °C range (*see* Figure 3D and supplemnetary S4). The Results show that the adsorption amounts of proteins increased with increasing temperatures.

2.5. Tendency of Adsorption Isotherm of Biomolecules

In order to study the adsorption isotherm of proteins in an aqueous solution using mesobiocaptor monoliths, we applied the Langmuir isotherm model at equilibrium as a theoretical

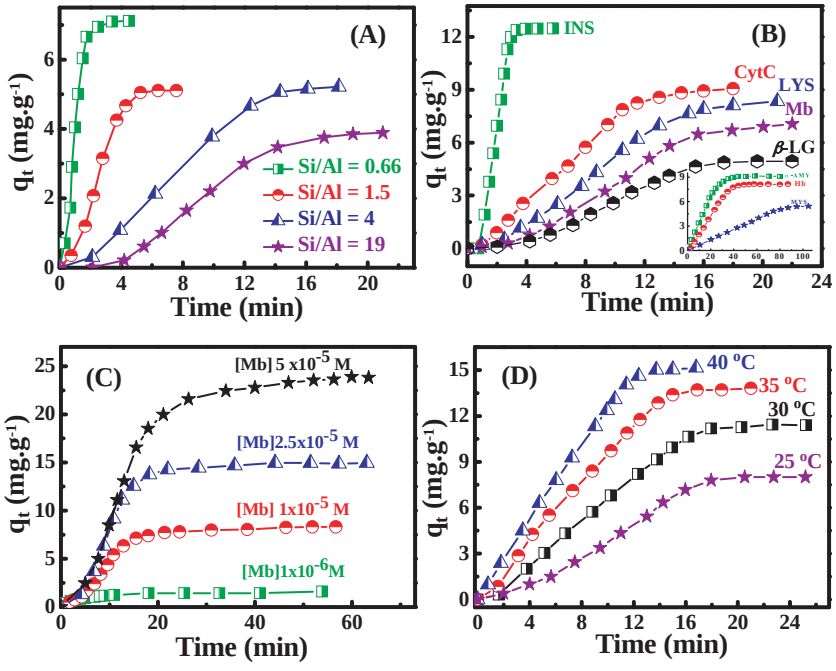

Figure 3. Time dependence of adsorption amount of proteins (q_t, $mg.g^{-1}$) onto biocaptors based on monoliths: (A) study the effect of Si/Al ratios of mesobiocaptors (1.6 g/L) on the adsorption process of (1×10^{-5} mol/L) Mb at 25 °C. (B) Effect of molecular weight, and size of (1×10^{-5} mol/L) proteins on adsorption assays using (1.6 g/L) mesobiocaptors with Si/Al ratio of 0.66 at 20 °C; (C) Effect of concentration range of Mb protein on adsorption assays using (1.6 g/L) mesobiocaptors with Si/Al ratio of 0.66 at 25 °C; and (D) effect of temperature on adsorption of (1×10^{-5} mol/L) Mb using mesobiocaptors with Si/Al ratio of 0.66.

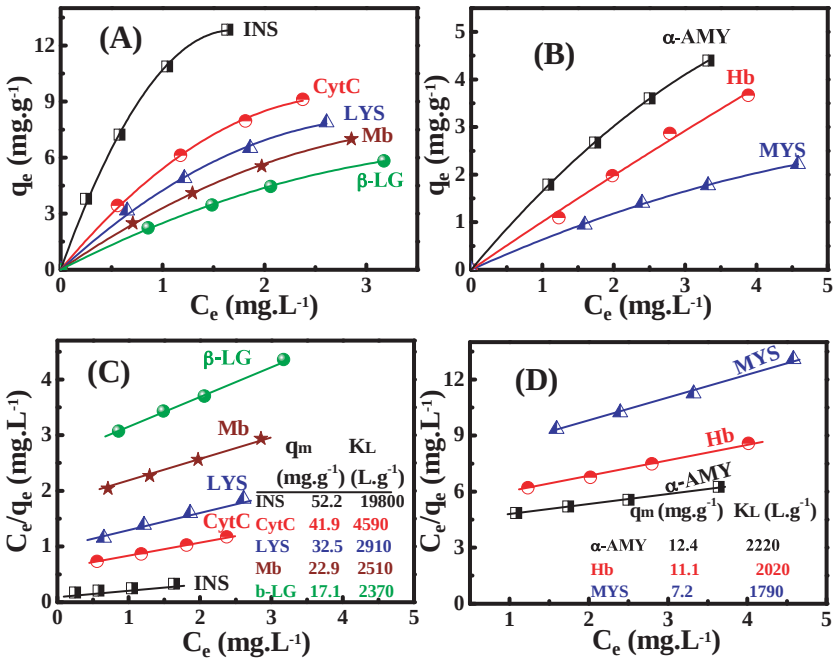

Figure 4. Langmuir adsorption isotherms (A and B) and the linear form of the Langmuir plot (C and D) for the adsorption of proteins into (1.6 g/L) mesobiocaptor with Si/Al of 0.66 at 25 °C. Inserts (C, D) are the q_m and K_L values of the protein adsorption assays.

model for monolayer adsorption. The monolayer coverage of proteins onto biocaptor surfaces at constant temperature is represented by the Langmuir isotherm (**Figure 4**). Results reveal the increase in the adsorption amount of mesobiocaptor monoliths with increasing concentration at equilibriums (Figure 4A and 4B). The straight line of the C_e/q_e versus C_e plot of this adsorption assay (Figure 4C and 4D) is evidence of the formation of monolayer coverage of proteins in the interior pore surfaces of monoliths. The linear adsorption curves indicate that a wide range of concentrations of biomolecules can be removed from aqueous water in a one-step treatment. A linear graph (Figure 4C and 4D) with a correlation coefficient range of 0.98 to 0.99 clearly showed that Langmuir adsorption isotherms characterized the adsorption assays for all proteins. The monolayer adsorption capacity, q_m, and the Langumir coverage constant, K_L, were obtained from the slope and the intercept of the linear plot. The q_m and K_L values decreased in the following order: MYS < Hb < α-AMY< β-LG < Mb < LYS < CytC < INS. This tendency is consistent with the adsorption behavior of these biomolecules.

2.6. Diffusivity of Biomolecules into Open Cylindrical Mesobiocaptors

The most commonly used mechanism for identifying the adsorption process is the intraparticle diffusion model. To understand the factors affecting the mass transport of the biomolecules from aqueous phase to the binding sites of the open cylindrical monoliths, the fractional attainment of equilibrium (f_e) against $t^{1/2}$ of mesobiocaptors was plotted at different sizes and shapes of proteins, according to Fick's second law relationship.[24,25] **Figure 5A** and **5B** show that S-curves that can be classified into three portions. The first linear portion reflects the instantaneous adsorption stage of proteins. During this step, the micrometric particles of the mesobiocaptors are considered as surrounded by a boundary layer of fluid film through which the protein might diffuse prior to external adsorption on the mesobiocaptor pore surfaces. The second curve portion signifies the intraparticle diffusion step into the open cylindrical pores of 16 nm, and the third portion is the final equilibrium stage. However, the intraparticle diffusion coefficient D is calculated from the slope of the second portion of Figure 5A and 5.[24–26] The results here indicate that the diffusion of the biomolecules across the aqueous diffusive boundary layer at the adsorbent-water interface might also affect the molecular transfer to the receiving adsorbent phase.[39,40] Such S-curve formation, in general, indicates that the intra-particle diffusion may control the mass transport of protein molecules from aqueous phase to the binding sites into the mesobiocaptor monoliths. Results reveal that the insertion of aluminum into the framework pores of monoliths might have enhanced the interior biomolecule-pore interactions.

In order to investigate the effect of molecular weight, size, and concentration of proteins on the coverage pore surface of mesobiocaptor within the interior diffusivity, the fraction of the coverage mesobiocaptor pore surfaces (f_c, g/m^2) occupied by the protein molecules were determined (Figure S5). Coverage surfaces f_c of proteins were significantly affected by active functional acid sites. Figures 5 show evidence that the fc and D parameters of the mesobiocaptors decreased in the following order: MYS < Hb < α-AMY< β-LG < Mb < LYS < CytC < INS. Based on these adsorption parameters, the lower adsorption effectiveness of these proteins was clearly consistent with the high molecular weight and concentrations of proteins.

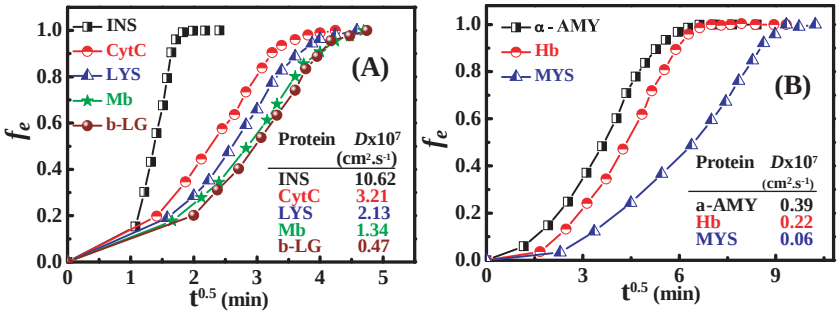

Figure 5. Fractional attainment of equilibrium (f_e) of (1.6 g/L) of mesobiocaptors (with Si/Al ratio of 0.66) at different sizes and shapes of proteins at 25 °C. Inserts (A, B) are the intraparticle diffusion coefficient D of the protein adsorption assays.

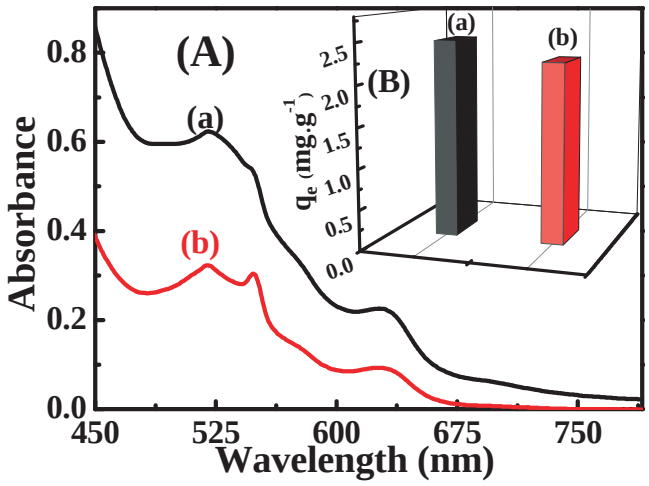

Figure 6. Absorbance studies (A) with size-selective adsorption assays of a (CytC and Hb) mixture of proteins with concentration of 2.5×10^{-5} mol/L per each protein by using (1.6 g/L) mesobiocaptors with Si/Al ratio of 4 (pore size of 4.8 nm) at 25 °C. Inserts (B), the amount adsorbed at equilbirium (q_e, mg.g^{-1}) of (2.5×10^{-5} mol/L) CytC in single (a) and (CytC and Hb) mixture (b) assays at 25°C.

2.7. Size-Selective Adsorption of Biomolecules

Our findings reveal that the size and shape of the each protein molecules played an important role in the adsorption process of protein molecules. However, proteins with main molecular sizes of ≤ 4 and 7 nm (INS size ≈ 2.4, CytC ≈ 3.0 nm, LYS ≈ 3.3 and β-LG size ≈ 4.2 nm) and (α-AMY ≈ 6.8 and Hb ≈ 7 nm) could be effectively adsorbed into mesocylindrical biocaptors fabricated with Si/Al ≤ 4 and 1.5 (i.e., with pore size of ≤ 4.8 and ≤ 8.4 nm, respectively) (Figure 1B). Large biomolecules, such as MYS (size ≥14 nm) were restrictively adsorbed into meso-biocaptor-fabricated Si/Al ≤ 0.66 (i.e. with pore size of 16 nm). We must note that the fabricated mesocylindrical biocaptors with Si/Al ratio of 19 (pore size of 3.3 nm) only adsorbed INS protein.

To illustrate the role of the pore size of mesobiocaptors in the efficiency of adsorption assays in terms of adsorption rate and diffusivity of macromolecules, size-selective adsorption assays of a mixture of proteins (CytC and Hb) by mesobiocaptors with Si/Al ratio of 4 (pore size of 4.8 nm) was applied. Spectroscopic analysis of the model proteins in a binary mixture suggests that small changes might have occurred in the protein structures (**Figure 6**). Due to the interaction affinity "heterocoagulation" of the protein particles in a binary mixture, growth of the proper protein sizes might have occurred, leading to enhanced adsorption time of proteins sized < 4 nm, such as CytC. However, the large-molecular-weight and -size Hb protein might be accumulated and blocked into the pore openings due to the low hydrodynamic hindrance of Hb compared with CytC proteins.[32,41,42] This finding indicates that the pore opening size is the key component for the size-selective separation of proteins.

2.8. Theoretical Models for Interior Immobilization of Proteins

To clarify the interior immobilization of proteins during the adsorption assays of mesobiocaptors, the cubic *Pm3n* aluminosilica monoliths outer and pore wall surface were analyzed to generate active receptor surface using protein soft-docking algorism implemented on SYBYL-X suite program.[43] This method was originally developed for protein/ligand and protein–protein docking. Therefore, we modified the code for solid adsorbent/protein docking according to our mesobiocaptor design based on 3D cubic networks. Various chemical properties, namely, charge, electrostatic potential, and hydrophobicity, were calculated to find the most stable configurations of the surface/protein-docking model. The crystal structure of hemoglobin (PDB ID: 2W72) was used as a model case for docking with our theoretical aluminosilica mesobiocaptor model. To compare the activity of outer and inner pore wall surfaces, several active spheres (with radii of 25 Å) on the aluminosilica model were defined, wherein the protein was docked in each sphere separately. Energy-wise, the most favorable configuration of the docked structure was selected in each docked model. **Scheme 3** summarizes the energies for most stable docked models. The

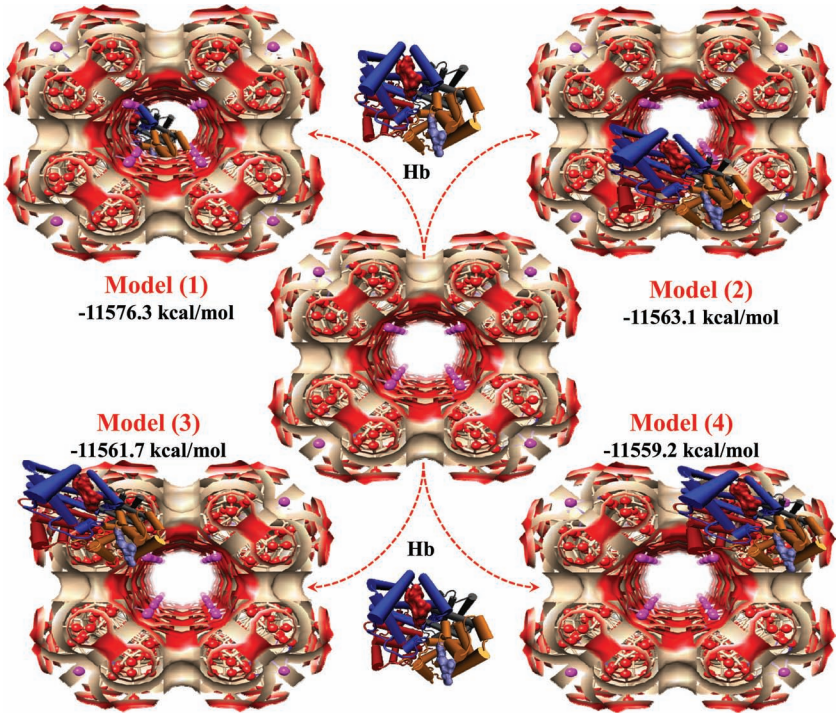

Scheme 3. Theoretical adsorption models of hemoglobin/aluminosilica mesobiocaptors generated by soft docking. Hemoglobin crystal structure was extracted from the protein data bank; the aluminosilica model was designed using quantum mechanics.

scheme shows that the model with protein oriented inside the pore (**Model 1**) is more stable by 10 *kcal/mol* smaller than any docked models in the outer pore surface. This result reflects the attraction between proteins and the active acid sites in the micrometer-sized particle of monoliths, which draws the proteins to diffuse toward the particle pore centers.

2.9. Reusability of Mesobiocaptor Monoliths

The limit applications of synthesized biocaptors in medicine are due to their low pore density and non-uniform pore size within reuse cycles. A major advantage of biocaptor monoliths is their reducibility and reversibility after multiple cycles of adsorption. Figure S8 shows that the monoliths retain high protein adsorption efficiency after a number of reuse cycles (i.e., dead-end adsorption).[27,35] Due to the difficulty of the clogging pores with proteins, Schmuki et al. reported a self-cleaning process to overcome the clogging of membrane pores by macromolecules.[20] In the current work, a simple chemical treatment based on acidified solution (HCl/NaCl) was used to effectively remove the trapped proteins in the monolith pores without significant damage in the textural and physical properties of the mesostructures. Our experimental findings show that, during the cleaning process, proteins with high molecular size and weight take longer to be removed from the interior of the monoliths (**Figure 7**). In addition, the large molecular sizes of proteins such as MYS and Hb lead to higher pore caking within the reuse/cycles compared to that of the smaller-molecular-sized proteins. Therefore, the efficiency of the monoliths during the reuse cycles of adsorption assays of proteins decreased in the order of MYS < Hb < α-AMY < β-LG < Mb < LYS < CytC < INS, indicating the effectiveness of the protein size, shape and weight in the continuous dead-end adsorption. Although the adsorption efficiency drastically decreased with cycling number, the reused mesobiocaptors remained effective, to some extent, for the protein adsorption after six recycles

3. Conclusion

We developed ultra- or micrometer-size-scale morphologies composed of 3D tube-shaped mesoporous monoliths, which could be used effectively to realize micro-objects tailored to a given protein encapsulation design. However, mesobiocaptor-based cubic *Pm3n* aluminosilica monoliths with open, large cylindrical pores of 16 nm could be fabricated using the stirring-assisted approach of microemulsion phases. Several key factors, such as molecular shape and size, concentration, and composition of proteins, in addition to the amount of active surface sites of monoliths, might control the potential immobilization of the proteins during the adsorption assays in terms of interior diffusivity and adsorption capacity. Our findings reveal that the pore sizes of mesobiocaptors play key roles in the efficiency of size-selective adsorption assays, particularly for separation of protein from a mixture. In the current work, geometrical models of the 3D mesobiocaptors were studied for the first time to investigate the major driving forces for the optimal performance of encapsulation/adsorption process in terms of diffusivity and quantity, particularly with large molecular weight, size, and concentrations of proteins. Our thermodynamic studies featured the stability of the protein immobilization into the interior pores of mesobiocaptors. This result reflects the attraction between proteins and the active acid sites in the micrometer-sized particles of the monoliths, which draws the proteins to diffuse toward the particle center. Although optimizing the reducibility and reversibility of the adsorbents remain a unique and interesting challenge, the protein adsorption efficiency by monoliths was attained after a number of reuse cycles, indicating the significant dead-end porosity of the biocaptor monoliths. The successful design of protein separation using such mesoporous materials might show promise in bioanalytical applications. Indeed, the proposed mesobiocaptor design might open up new avenues of research for the availability of complete removal of single protein from mixtures based on size- and shape-selective separation, leading to the study of the structures of all proteins from a single organism or comparing, across many different species, proteins that play a specific biological role.

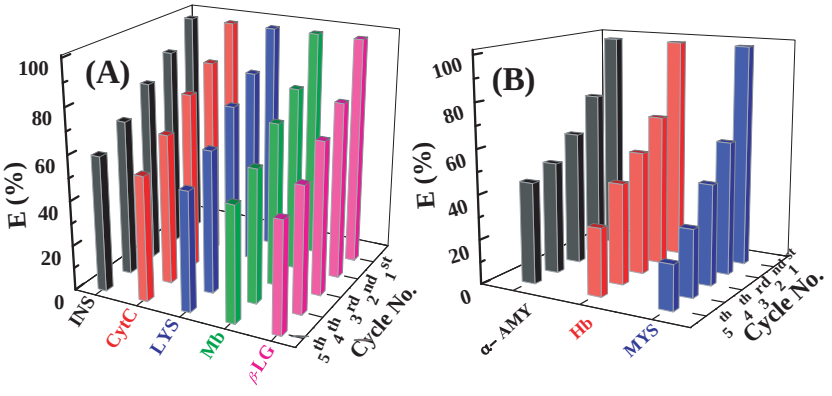

Figure 7. Reusability study of the (1×10^{-6} M) protein adsorption into (1.6 g/L) meso-biocaptor with Si/Al ratio of 0.66 and at 25 °C. The efficiency (E%) of the meso-biocaptor was calculated from the% ratio of recovery adsorbed amount of protein at equilibrium (q_r) per reuse cycle (No.) and the initially adsorbed amount (q_o) obtained from the initial use of the meso-biocaptor monoliths.

4. Experimental Section

Synthesis of Mesoporous Aluminosilica with Micrometer-Sized Biocaptors: Stirring-assisted direct-template synthesis was used to fabricate large cylindrical mesopore aluminosilicas with different Si/Al molar ratios (19 < Si/Al < 0.66) and micrometer-sized monolith particles. Controlled cubic *Pm3n* aluminosilica mesostructures with low Si/Al ratio contents ≥ 0.66 were synthesized by using a direct templating method of quaternary microemulsion liquid crystalline phases of Brij 58/C_{12}-alkane/TMOS/H_2O-HCl/ethanol composition. For example, the direct synthesis of cubic *Pm3n* aluminosilica at Si/Al molar ratio of 4 with TMOS/Brij-58 mass ratio of 0.5 (w/w), the precursor solution [1 g of Brij-58, 0.5 g of dodecane, 2 g of TMOS, 1.26 g of $Al(NO_3)_3$, 2.5 g of H_2O-HCl (pH 1.3), and 10 g ethanol] was stirred for 5 min to form a homogenous sol-gel solution. The mass ratio of surfactant to dodecane was kept at 2:1 for all syntheses of the mesoporous aluminosilica. To

obtain samples with aluminum content at Si/Al ratios of 19, 4, 1.5 and 0.66, the composition of $Al(NO_3)_3$ was varied from 0.7×10^{-3} to 20.61×10^{-3} mole ratios. As the hydrolysis/condensation reactions continued during the stirring for 2 h, the liquid viscosity of the material increased, and the resulting optical gel-like material acquired the shape and size of the reaction vessel. The solid material was allowed to dry completely at 40 °C overnight. The organic moieties were removed by calcination at 550 °C in air for 5 h.[22]

Batch Adsorption Method of Organic Pollutants: The batch adsorption of the insulin (INS, 5.733 kDa, 2.4 nm), cytochrome C (CytC, 12,327 kDa, 3.0 nm), lysozyme(LYS, 14,300 kDa, 3.2 nm), myoglobin (Mb, 16,950 kDa, 4.0 nm), β-lactoglobin (β-LG, 18.4 kDa, 4.2 nm), α-amylase (α-AMY, ~54 kDa, 6.8 nm), hemoglobin (Hb, 68.000 kDa, 7.0 nm) and myosin (MYS, 200–500 kDa, ~14–19 nm) proteins using (0.05g) mesobiocaptor monoliths was performed in an aqueous solution (30 mL) under constant stirring and at different temperatures (25 °C to 40 °C, ±0.1 °C range). The initial concentration used of proteins was in the range of 1×10^{-6}mol/L to 5×10^{-5} mol/L. Afterwards, the protein aliquots were collected and monitored as a function of exposure time. The concentration of LYS and β-LG proteins were studied using fluorescence spectroscopy (PerkinElmer LS45) at $\lambda_{emission}$ of 350 and 342 nm, respectively, with excitation wavelengths of 292 and 290 nm, respectively. However, the concentration of INS, CytC, LYS, Mb, Hb, AMY, and MYO proteins were studied using UV–Vis spectroscopy (a Shimadzu 3700 model solid-state) at λ of 277, 409, 408, 405, 252, and 267 nm. The decrease of the UV-Vis and fluorescence spectra of all proteins at specific wavelengths indicated the adsorbed amount of proteins inside the mesocylindrical biocaptors within these adsorption processes.

Supporting Information

Supporting Information is available from the Wiley Online Library or from the author.

Received: February 8, 2012
Revised: March 13, 2012
Published online: April 24, 2012

[1] Z. Liu, M. Li, X. Yang, M. Yin, J. Ren, X. Qu, *Biomaterials* **2011**, *32*, 4683–4690.
[2] I. S. Lee, N. Y. Lee, J. Park, B. H. Kim, Y. W. Yi, T. Kim, *J. Am. Chem. Soc.* **2006**, *128*, 10658–10569.
[3] H. M. Chen, C. H. Deng, X. M. Zhang, *Angew. Chem. Int. Ed*. **2010**, *49*, 607–611.
[4] S. S. Liu, H. M. Chen, X. H. Lu, C. H. Deng, X. M. Zhang, P. Y. Yang, *Angew. Chem. Int. Ed*. **2010**, *49*, 7557–7561.
[5] J. D. Andrade, V. Hlady, A. P. Wei, *Pure & Appl. Chem.* **1992**, *64*, 1777–1781.
[6] J. D. Andrade, V. Hlady, *Ann. N. Y. Acad. Sci.* **1987**, *576*, 158.
[7] F. Bellezza, A. Cipiciani, L. Latterini, T. Posati, P. Sassi, *Langmuir* **2009**, *25*, 10918–10924.
[8] J. Deere, E. Magner, J. G. Wall, B. K. Hodnett, *Catal. Lett.* **2003**, *85*, 19.
[9] M. Mahato, P. Pal, T. Kamilya, R. Sarkar, G. B. Talapatra, *J. Phys. Chem. B* **2010**, *114*, 495–502.
[10] T. Stroink, G. Wiese, J. Teeuwsen, H. Lingeman, J. C. Waterval, A. Bult, G. J. Jong, W. J. Underberg, *Electrophoresis* **2003**, *24*, 897–903.
[11] M. Gilar, Y-Q. Yu, J. Ahn, J. Fournier, J. C. Gebler, *J Chromatogr A* **2008**, *1191*, 162–170.
[12] J. Villanueva, J. Philip, D. Entenberg, C. A. Chaparro, M. K. Tanwar, E. C. Holland, P. Tempst, *Anal Chem*. **2004**, *76*, 1560–1570.
[13] W. Jia, X. Chen, H. Lu, P. Yang, *Angew. Chem. Int. Ed.* **2006**, *45*, 3345–3349.
[14] Z. Xu, S-L. Wang, H-W. Gao, *J. Hazard. Mater.* **2010**, *180*, 375–383.
[15] S. B. Hartono, S. Z. Qiao, K. Jack, B. P. Ladewig, Z. Hao, G. Q. Lu. *Langmuir* **2009**, *25*, 6413–6424.
[16] C. Wang, S. Tao, W. Wei, C. Meng, F. Liu, M. Han, *J. Mater. Chem.* **2010**, *20*, 4635–4641.
[17] T-Y. Ma, X-J. Zhang, Z-Y. Yuan, *J. Phys Chem. C.* **2009**, *113*, 12854–12862.
[18] C. T. Kresge, M. E. Leonowicz, W. J. Roth, J. C. Vartuli, J. S. Beck, *Nature* **1992**, *359*, 710–712.
[19] F. Hoffmann, M. Cornelius, J. Morell, M. Fröba, *Angew. Chem. Int. Ed*. **2006**, *45*, 3216–3251.
[20] S. A. El-Safty, Y. Kiyozumi, T. Hanaoka, F. Mizukami, *J. Phys. Chem. C* **2008**, *112*, 5476–5489.
[21] J. R. Matos, M. Kruk, L. P. Mercuri, M. Jaroniec, L. Zhao, T. Kamiyama, O. Terasaki, T. J. Pinnavaia, Y. Liu, *J. Am. Chem. Soc.* **2003**, *125*, 821.
[22] F. Kleitz, D. Liu, G. M. Anilkumar, I. Park, L. A. Solovyov, A. N. Shmakov, R. Ryoo, *J. Phys. Chem. B* **2003**, *107*, 14296.
[23] R. Tian, H. Zhang, M. Ye, X. Jiang, L. Hu, X. Li, X. Bao, H. Zou, *Angew. Chem. Int. Ed*. **2007**, *46*, 962–966.
[24] S. A. El-Safty, Y. Kiyozumi, T. Hanaoka, F. Mizukami, *Appl. Catal., A* **2008**, *337*, 21.
[25] P. A. Mangrulkar, S. P. Kamble, J. Meshram, S. S. Rayalu, *J. Hazard. Mater.* **2008**, *160*, 414.
[26] J. X. Lin, S. L. Zhan, M. H. Fang, X. Q. Qian, *J Porous Mater.* **2007**, *14*, 449–455.
[27] S. A. El-Safty, T. Hanaoka, *Adv. Mater.* **2003**, *15*, 1893.
[28] A. E. Garcia-Bennett, K. Lund, O. Terasaki, *Angew. Chem. Int. Ed*. **2006**, *45*, 2434.
[29] S. A. El-Safty, A. Shahat, Md. R. Awual, *J. Colloid Interface Sci.* **2011**, *359*, 9–18.
[30] J. F. Díaz, K. J Balkus, *J. Mol. Catal. B Enzym* **1996**, *2*, 115–126.
[31] A. R. Garcia, R. B. de Barros, A. Fidalgo, L. M. Ilharco, *Langmuir* **2007**, *23*, 10164–10175.
[32] K. S. W. Sing, D. H. Everett, R. A. W. Haul, L. Moscow, R. A. Pierotti, J. Rouquerol, T. Siemieniewska, *Pure Appl. Chem.* **1985**, *57*, 603.
[33] S. A. El-Safty, F. Mizukami, T. Hanaoka, *J. Phys. Chem. B* **2005**, *109*, 9255.
[34] S. A. El-Safty, T. Hanaoka, F. Mizukami, *Adv. Mater*. **2005**, *17*, 47.
[35] D. Tang, R. Niessner, D. Knopp, *Biosens. Bioelectron.* **2009**, *24*, 2125–2130.
[36] S. A. El-Safty, T. Balaji, H. Matsunaga, T. Hanaoka, F. Mizukami, *Angew. Chem., Int. Ed.* **2006**, *45*, 7202.
[37] R. Mokaya, *Angew. Chem., Int. Ed.* **1999**, *38*, 2930.
[38] M. C. Chao, H. P. Lin, C. Y. Mou, B. W. Cheng, C. F. Cheng, *Catal. Today* **2004**, *97*, 81.
[39] T. Linssen, F. Mees, K. Cassiers, P. Cool, A. Whittaker, E. F. Vansant, *J. Phys. Chem. B* **2003**, *107*, 8599.
[40] N. A. Oladoja, C. O. Aboluwoye, Y. B. Oladimeji, A. O. Ashogbon, I. O. Otemuyiwa, *Desalination* **2008**, *227*, 190–203.
[41] M. Colilla, M. Manzano, M. Vallet-Regí, *Int. J. Nanomed.* **2008**, *3*, 403–414.
[42] J.-R. Ku, P. Stroeve, *Langmuir* **2004**, *20*, 2030–2032.
[43] SYBYL-X 1.2, Tripos International, 1699 South Hanley Rd., St. Louis, Missouri, 63144, USA.